Received: 13 October 2021 | Revised: 11 April 2022 | Accepted: 23 May 2022

DOI: 10.33012/navi.544

ORIGINAL ARTICLE

Commercial GNSS Radio Occultation on Aerial Platforms With Off-The-Shelf Receivers

Bryan C. Chan[1] | **Ashish Goel**[1] | **Jonathan Kosh**[1] | **Tyler G. R. Reid**[1] | **Corey R. Snyder**[1] | **Paul M. Tarantino**[1] | **Saraswati Soedarmadji**[1] | **Widyadewi Soedarmadji**[1] | **Kevin Nelson**[2] | **Feiqin Xie**[2] | **Michael Vergalla**[3]

[1] Night Crew Labs, CA, USA

[2] Dept. of Physical & Environmental Sciences, Texas A&M University Corpus Christi, TX, USA

[3] Free Flight Lab, CA, USA

Correspondence
Bryan C. Chan
Night Crew Labs, Woodside, CA, USA.
Email: bryan@nightcrewlabs.com

Abstract

In recent decades, GNSS radio occultation (RO) soundings have proven to be an invaluable input to global weather forecasting. The success of government programs such as COSMIC is now complemented by commercial low-cost cubesats. The result is access to more than 10,000 soundings per day. We examine aerial platforms for commercial GNSS-RO, specifically high-altitude balloons and commercial aviation. Meteorological balloons (radiosondes) are deployed daily in over 900 locations globally. Adding GNSS-RO capability to radiosondes would expand capability and enable local area monitoring. Commercial aviation offers scale with more than 100,000 flights daily. A barrier to entry for the inclusion of GNSS-RO sensors is cost and complexity, as GNSS-RO traditionally requires highly specialized equipment. This paper describes a low-cost and scalable approach to aerial GNSS-RO based on commercial-off-the-shelf (COTS) GNSS receivers. We present hardware prototypes and data processing techniques that demonstrate technical feasibility through the results from several flight testing campaigns.

Keywords

COTS, GNSS-RO, high-altitude balloon (HAB), radio occultation

1 | INTRODUCTION

GNSS radio occultation (RO) leverages GNSS satellites rising and setting on the horizon to extract refractivity in the troposphere and the ionosphere. Traditionally, highly specialized scientific instruments have been deployed on low-Earth-orbiting (LEO) platforms to collect GNSS-RO soundings where the first LEO GPS-RO experiment was performed in 1995 by the Microlab 1 satellite (Ware et al., 1996). Subsequently, there have been numerous successful missions that utilize GNSS signals for atmospheric and ionospheric soundings (Yue et al., 2011). The joint U.S.-Taiwan Constellation Observing System for Meteorology, Ionosphere, and Climate (COSMIC) was launched in 2006 and represents the first dedicated LEO constellation of six satellites employing GNSS-RO techniques (Anthes et al., 2008; Kumar, 2006). The success of COSMIC demonstrated the operational value of these soundings in weather prediction, space weather monitoring, and geodesy.

The system's second generation, COSMIC-2, was launched in 2019 with the goal of generating nearly 5,000 RO soundings per day (Schreiner et al., 2020) compared to COSMIC-1's 1,000–2,000 (Feltz et al., 2017; Yue et al., 2014).

Missions like COSMIC represent a highly specialized approach to GNSS-RO, creating unique scientific instruments for GNSS-based atmospheric soundings. Others have taken a new space approach to GNSS-RO, one characterized by nanosatellites and commercial-off-the-shelf (COTS) components. In 2008, the 3U cubesat known as the Canadian Advanced Nanosatellite Experiment-2 (CANX-2) mission was launched with a COTS GPS receiver to perform just such an experiment (Kahr et al., 2011, 2013; Sarda et al., 2009). This showed that useful ionospheric soundings could be attained with a cost two orders of magnitude less compared to COSMIC (Swab, 2015). The Cascade, Smallsat, and Ionospheric Polar Explorer (CASSIOPE) satellite launched in 2013 further showcased the capability of COTS receivers for GNSS-RO (Shume et al., 2015). Building on this work, GNSS-RO methods for cubesat missions were expanded and now make up a large commercial enterprise producing more than 10,000 RO soundings per day (Bowler, 2020; Irisov et al., 2020; Skone et al., 2014). These data products are utilized in weather prediction by the U.S. National Oceanic and Atmospheric Administration (NOAA) and U.S. Air Force (USAF) along with various other global weather and research groups (Irisov et al., 2020). This commercial success showcases the value of such data and that there is a continued appetite for more soundings with NOAA targeting 20,000 ROs per day (Werner, 2020), tenfold more than what was available just a short time ago.

This has resulted in further interest in commercially deploying GNSS-RO on complementary platforms. Here, we examine an underutilized platform for GNSS-RO: the high-altitude weather balloon. Balloon platforms were first examined for GPS-RO by Haase et al. (2012), showing feasibility and scientific proof of concept. Here, we further explore concepts for commercialization and widescale deployment. Meteorological radiosondes (weather balloons) are deployed twice daily in over 900 locations globally and form an essential in-situ data source as a long-standing input to weather forecasting models. In fact, these platforms are often used as ground truth for the development of new GNSS-RO techniques and for calibration (Kuo et al., 2005). Adding GNSS-RO capability to existing radiosonde platforms would greatly expand capability, allowing for persistent and local area monitoring—a feature particularly useful for hurricane and other severe weather monitoring. A prohibitive barrier of entry to this inclusion is cost and complexity as GNSS-RO traditionally requires highly specialized equipment. This paper describes a multi-year effort to develop a low-cost and scalable approach to balloon GNSS-RO based on COTS GNSS receivers.

Challenges with commercial GNSS receivers on high-altitude balloon platforms were first examined by the authors with test flights in 2011 (Carroll et al., 2011). The proof of concept for COTS-based GNSS-RO from high-altitude balloons was first flown by the authors in 2018 (Chan et al., 2018). With the development of retrieval algorithms, it was shown that quality GNSS-RO soundings can be gathered by such a system (Chan et al., 2019). This proof of concept formed the foundation for our research. This paper will present hardware prototypes and data processing techniques that demonstrate the technical feasibility of the approach through results from several high-altitude balloon and fixed-wing aircraft flight testing campaigns.

2 | INSTRUMENTATION

The instrumentation to support these efforts can be broadly categorized into (a) science payloads for GNSS-RO and (b) mission systems support, which includes

mission management and data logging. This section will describe the mission management system known as the Balloon Reprogrammable Integrated Computer (BRIC) as well as two generations of COTS-based GNSS-RO science instruments. The first generation is named the GNSS Radio Occultation and Observable Truth (GROOT) system and represents the first COTS-based system developed for this application. The GROOT system evolved into the Aircraft In-Situ and Radio Occultation (AIRO) instrument for expanded capability in a smaller form factor–this evolution is key to transitioning this work from research to commercial operations.

2.1 | BRIC

The BRIC represents the third generation of the internally developed flight management computer to support Night Crew Labs' (NCL) high-altitude balloon (HAB) flights which date back to 2011 (Carroll et al., 2011). The BRIC's high-level functions are summarized in Figure 1. Figure 2 shows the hardware stack that represents a design based on an Arduino Mega 2560 for low power consumption and simplicity of implementation. Next on the stack is a custom printed circuit board (PCB) which houses various sensors and interfaces. This includes barometric pressure sensors, thermistors for both environmental characterization and closed-loop heating control, communication via an Iridium satellite link, and GPS for navigation. The GPS element of this stack was not used for radio occultation and was, rather, designed for system-level independence of the science instrument for mission reliability.

The BRIC further provides an interface to the power management system where current and voltage can be measured and subsystems can be commanded on or off as needed. Next in the stack are two COTS relay shields for control of high-power load functions, including individual electric heaters, ballast release, and flight termination. Ballast release consists of an actuated valve that releases a glycol-water mixture to maintain buoyancy over several night and day cycles. The flight termination system has a nichrome wire that can be heated to cut the payload paracord for controlled descent back to the ground under parachute. On the top of the stack, we have an SD card shield for data logging. These functions are summarized in Figure 1.

This system has been extensively tested both on the ground and in flight. A large part of the software and hardware were tested through previous generations on more than ten successful balloon flights. The specific changes for this campaign were extensively tested on the bench. Shown in Figure 3 is hardware-in-the-loop (HIL)

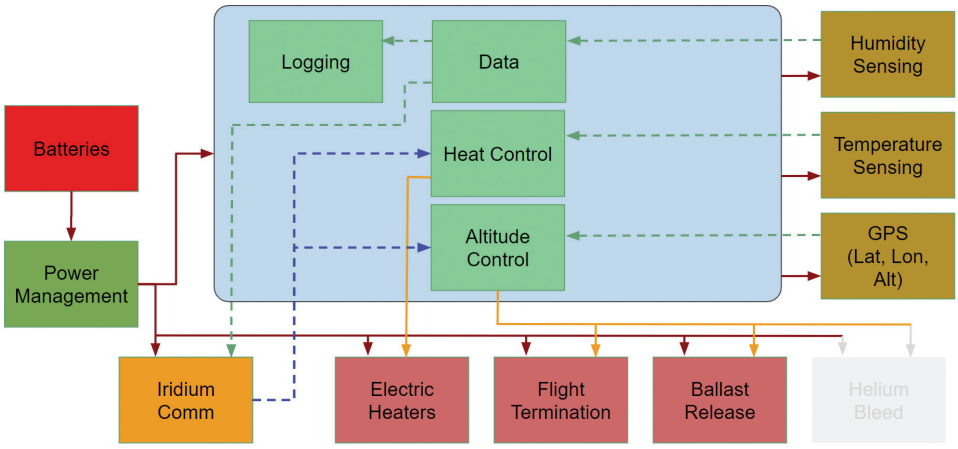

FIGURE 1 The BRIC flight management computer functional block diagram

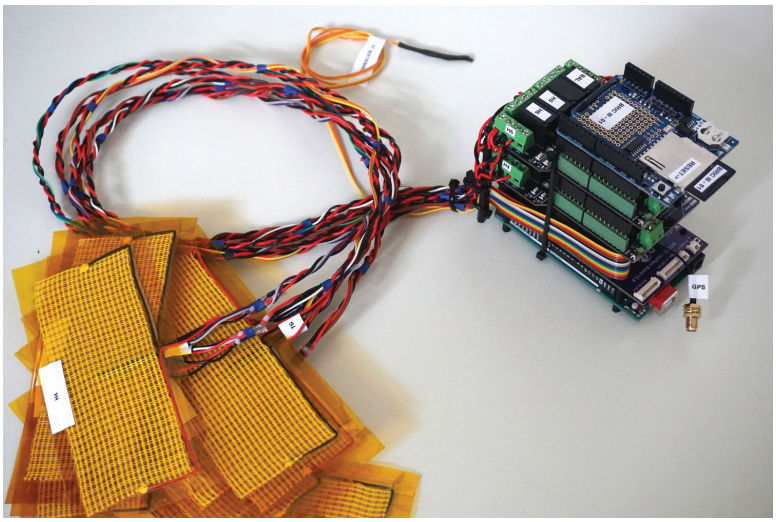

FIGURE 2 The BRIC flight management computer hardware that operates NCL HAB missions including navigation, communication, thermal management, and data logging

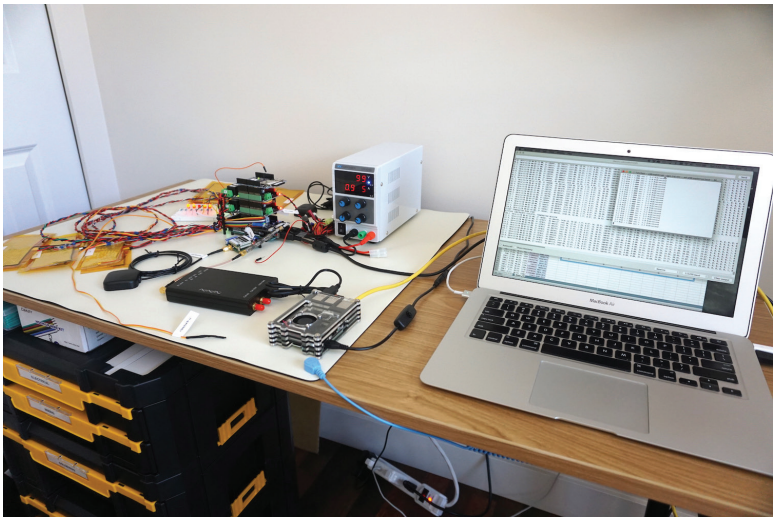

FIGURE 3 Hardware-in-the-loop testing of the BRIC flight computer; shown here is a GPS simulator running through a multi-day representative flight trajectory.

testing with a GPS simulator based on a software-defined radio (SDR). This example is running a multi-day representative flight trajectory to qualify system behavior.

The system connects using an Iridium satellite link to a custom ground station interface, where aspects of the mission can be commanded remotely via an internet browser. Functionality includes health and telemetry data, as well as the ability to shut down power to individual subsystems as needed. Perhaps most importantly, this includes multi-redundant flight termination capability in the event that winds suddenly change and it is deemed necessary to terminate the mission manually. Under nominal conditions, the system is intended to operate autonomously. These operations occur in quasi-real-time as data exchange between the ground and balloon payload is set to every 2 minutes. An example of the ground station interface and data telemetry is shown in Figure 4 and Figure 5, respectively.

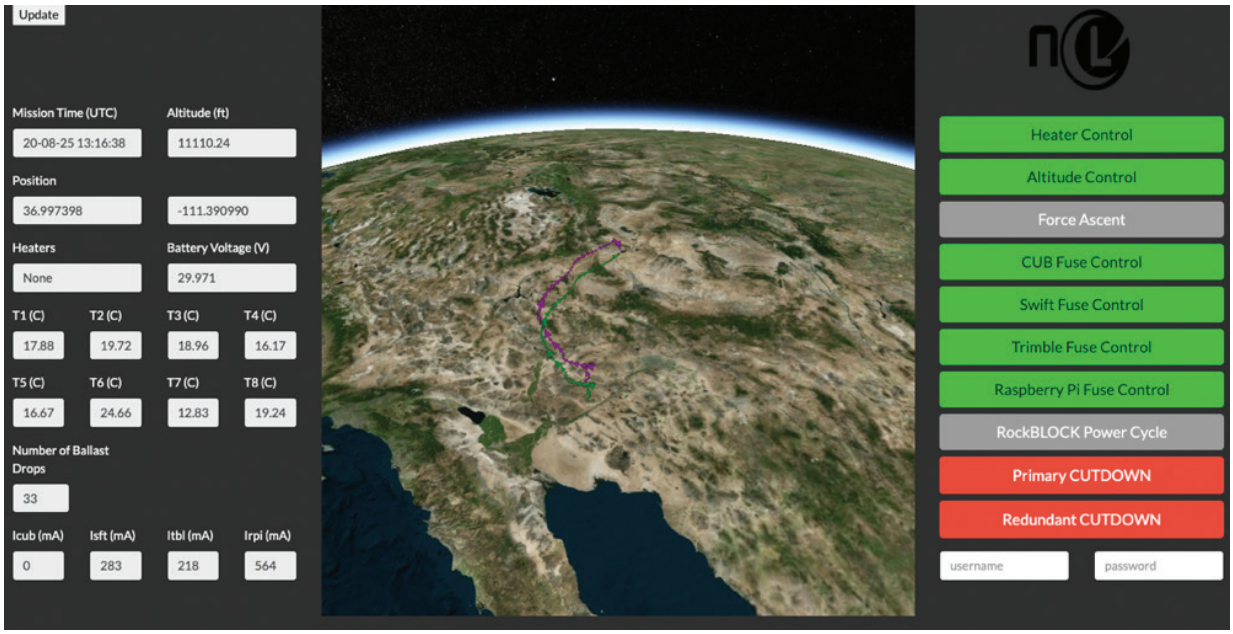

FIGURE 4 Custom browser-based ground station interface for balloon mission management; Iridium satellite connectivity allowed for command and control from anywhere in the world.

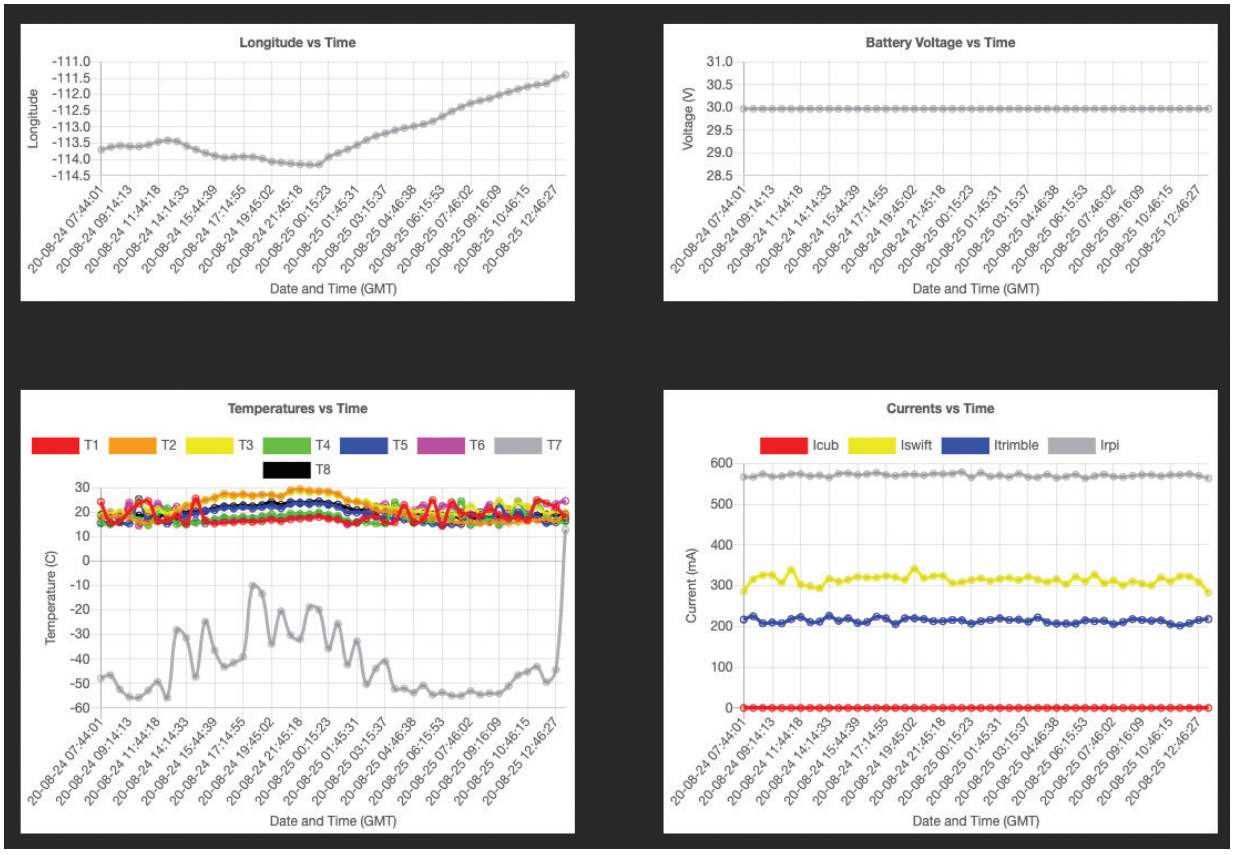

FIGURE 5 Ground station telemetry during flight including the position, battery voltage, internal/external temperatures, and equipment current draw

2.2 | GROOT

The GNSS Radio Occultation and Observable Truth (GROOT) system represents the first generation of GNSS-RO science instruments based on COTS GNSS equipment by Night Crew Labs. The intent of this instrument was to collect and log the data necessary for processing and extracting GNSS-RO soundings. This includes both the raw GNSS observables of the occulting satellite (e.g., carrier phase, signal-to-noise ratio [SNR], and Doppler) as well as a highly accurate position and velocity of the platform. To accomplish this, the GROOT system leveraged two separate GNSS devices.

Raw measurements for RO were collected by a stock Piksi Multi from Swift Navigation, a closed-loop tracking commercial receiver that can track up to 22 satellites simultaneously, specifically GPS L1/L2, GLONASS G1/G2, BeiDou B1/B2, and Galileo E1/E5b at up to 20 Hz. Precise position and velocity were computed using a dual-antenna GNSS + inertial Trimble BX992 with an L-band correction service for precise point positioning (PPP). Both receivers shared the same antenna—the Trimble AV39 designed for aviation. The Trimble BX992 further relied on a pair of AV39 antennas to aid the inertial navigation solution with GNSS-based heading.

Both the raw observables from the Piksi Multi and precise position and velocity from the BX992 were logged using a Raspberry Pi computer. Figure 6 shows the GROOT system alongside the BRIC in a pre-flight assembly. Both GNSS units leveraged the same set of antennas, hence the need for the GNSS antenna splitters to be shown in assembly. A functional block diagram of the GROOT system is shown in Figure 7.

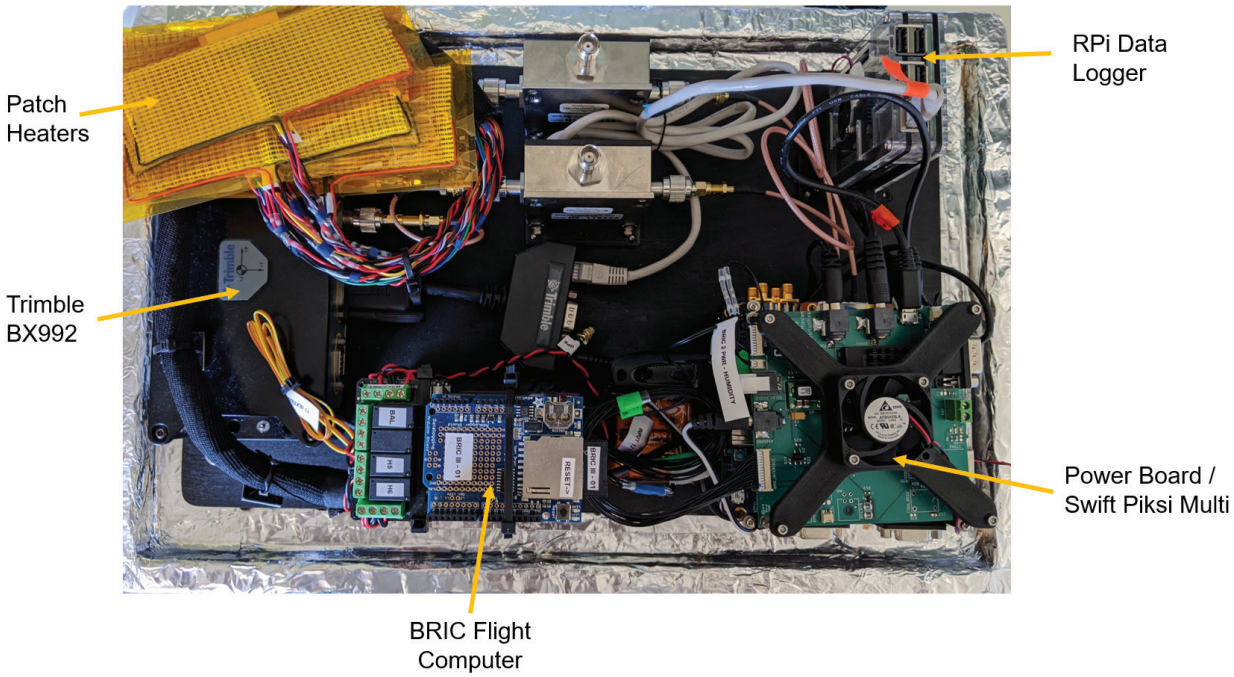

FIGURE 6 The GROOT system; a SwiftNav Piksi Multi recorded RO measurements, a Trimble BX992 generated precise position and velocity, and the data was logged to a RPi computer.

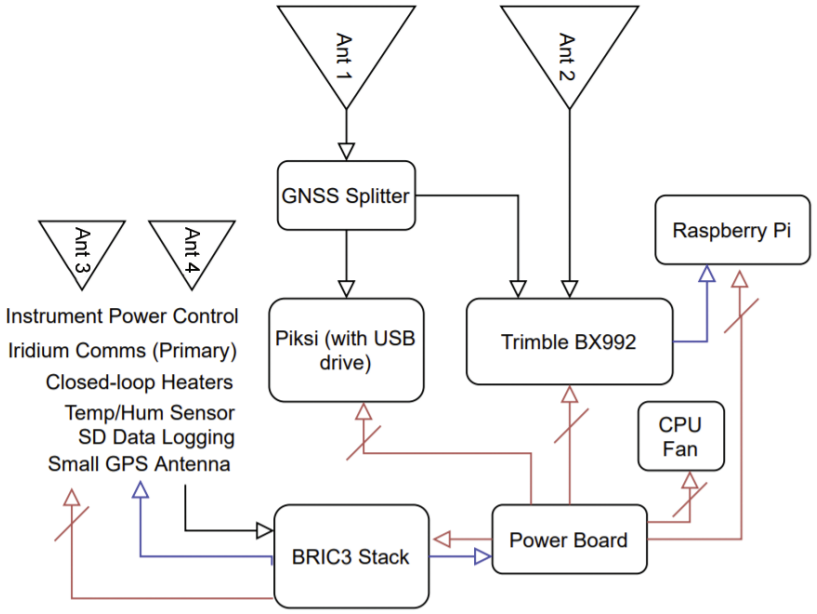

FIGURE 7 The GROOT-RO instrument functional block diagram

2.3 | AIRO

The GROOT system evolved into the Aircraft In-Situ and Radio Occultation (AIRO) instrument. The goal of AIRO was to reduce the cost, size, weight, and power (CSWaP) of the GROOT proof of concept while maintaining RO data quality. This represents a major step towards a form factor appropriate for widespread deployment and commercialization.

As is discussed in Section 4, COTS GNSS receivers prove highly capable in producing data of sufficient quality for RO vertical profile retrieval. Continuing this trend, the requirements for the AIRO instrument to select the most appropriate COTS GNSS device were that the receiver be capable of outputting raw GNSS observables at a high rate, track signals below the horizon, produce a highly accurate position and velocity solution, as well as have a small form factor and relatively low cost. As a result, the Septentrio Mosaic series was selected, capable of outputting all necessary measurements and providing a high-accuracy position/velocity solution with optional L-band correction capability.

Satellite-based PPP corrections are necessary in HAB applications as they often fly out of the sight of cellular networks. As the ultimate goal is to process RO measurements in quasi-real-time onboard the balloon, L-band corrections have become a necessity. A prototype was developed based on the mosaicHat, an open-source design that interfaces the Mosaic X5 to a Raspberry Pi 4 computer (Sa'd, 2020). The design rendering is shown in Figure 8 and the assembled functional prototype is shown in Figure 9. With correction services enabled, there is the potential for this to serve as both the ground truth and RO instrument, greatly reducing the size and complexity going forward. This also reduces processing complexity, reducing the steps required for calibration between two separate GNSS systems. Though the device is L-band correction services capable, no such service has yet been utilized in our experiments.

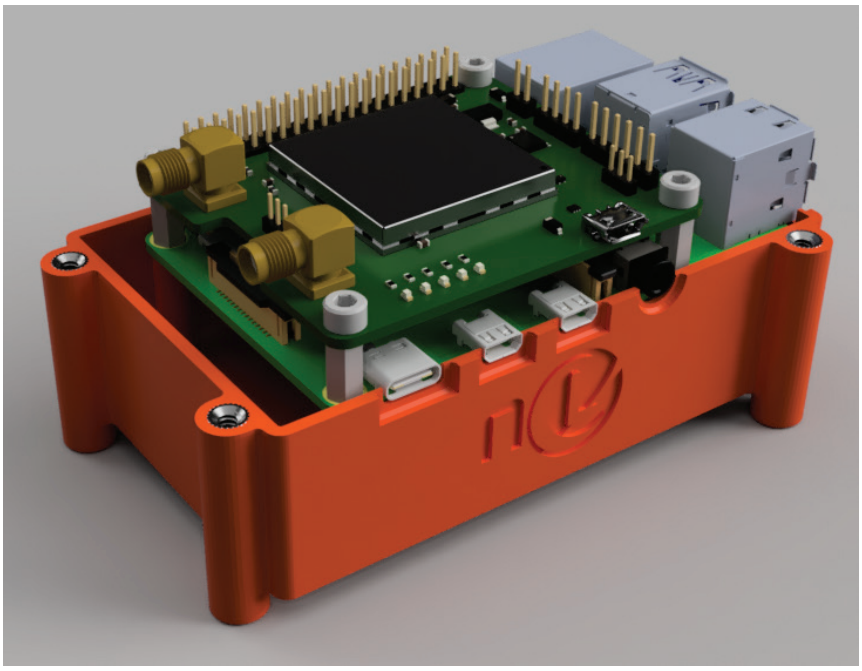

FIGURE 8 3D rendering of the AIRO instrument based on the mosaicHat and Raspberry Pi 4

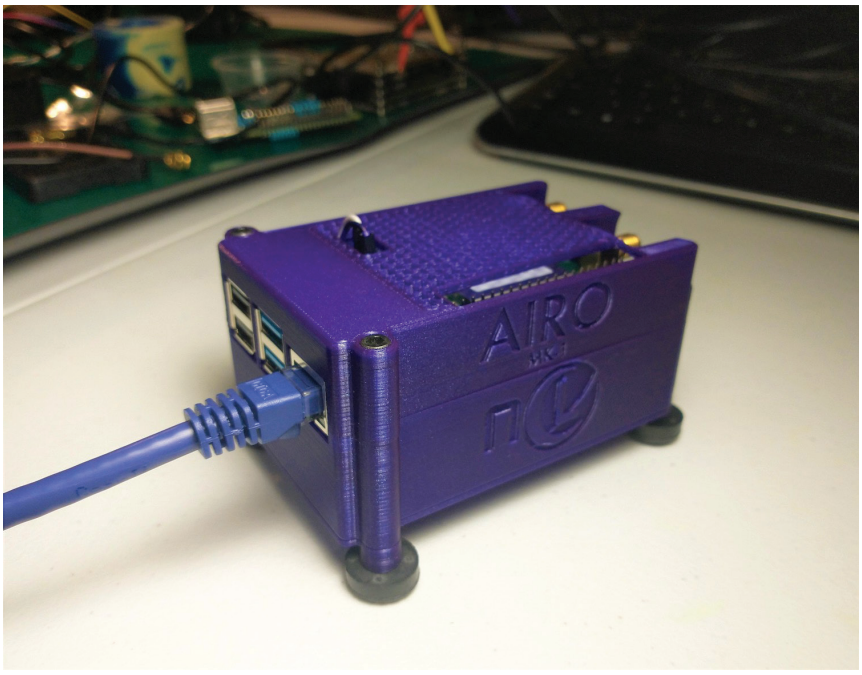

FIGURE 9 Completed functional prototype of the AIRO instrument

3 | FLIGHT TEST CAMPAIGNS

More than ten total flight tests took place over the course of 2020 on three distinct aerial platforms. These campaigns are summarized in Table 1. In this section, we describe seven fixed-wing aircraft flights along with three HAB flights, representing more than 150 hours of flight testing with the GROOT system.

TABLE 1
Summary of Flight-Testing Campaigns

Platform	Number of Flights	Total Hours
Beechcraft King Air Research Aircraft (Univ. of Wyoming)	7	21
World View Long Duration Balloon	2	120
Night Crew Labs Zero Pressure Balloon	1	12

3.1 | Beechcraft King Air

The first of these campaigns took place on a fixed-wing research aircraft platform in collaboration with Airbus Silicon Valley and the University of Wyoming in February 2020. This was undertaken on a Beechcraft King Air research aircraft shown in Figure 10. This entailed eight flights using the King Air over six days, collecting over 21 hours of data. The data collection setup is shown in Figure 11. The cruising altitude was 8 km (26,000 ft).

FIGURE 10 King Air research aircraft at the University of Wyoming

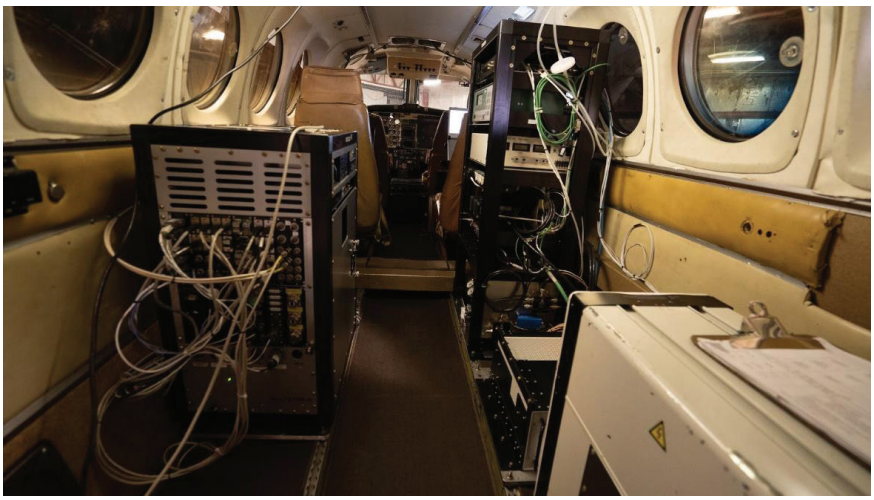

FIGURE 11 Instrumentation setup in the King Air research aircraft; this shows several data collection systems in which the GROOT system was only a 1U form factor in the equipment rack.

3.2 | World View Long-Duration Balloon Flight

Following the King Air campaign was the first series of high-altitude balloon flights in the summer of 2020. These were undertaken on zero-pressure balloons as a secondary hosted payload on the World View stratollite balloon bus platform shown in Figure 12. This involved two flights out of Page, Arizona, that maintained 18+ km (60,000+ ft) altitude, enabling five days (120 hours) of continuous data collection. The balloon launch is shown in Figure 13 and the Night Crew Labs instrumentation package is shown in Figure 6.

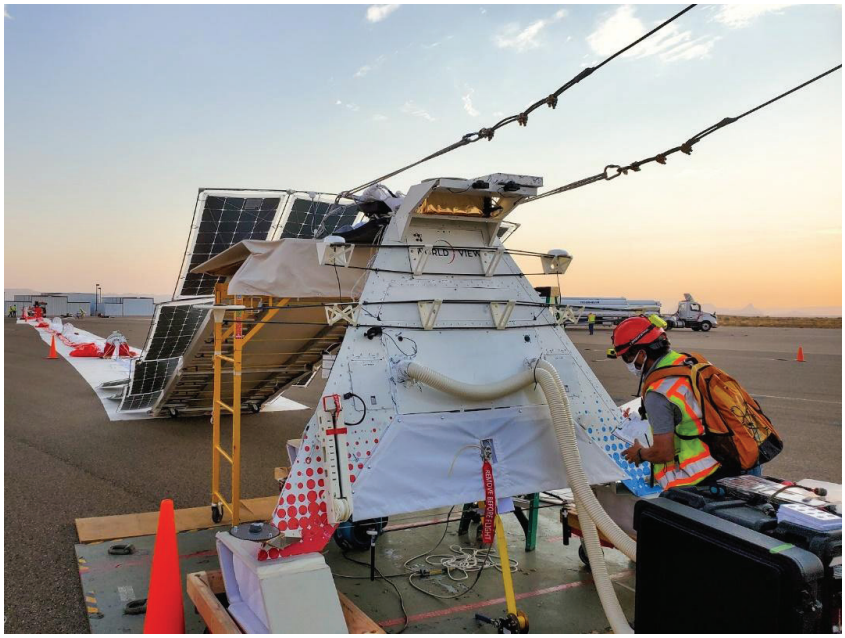

FIGURE 12 World View stratollite; the NCL GNSS-RO instrument was a hosted payload on the bottom face.

FIGURE 13 World View zero-pressure balloon on launch day being filled with helium

The Night Crew Labs' payload included both the science instrument for RO soundings (GROOT), as well as the mission management system (BRIC) complete with tracking, satellite communication for remote command and control, as well as thermal management and data loggers. During the flight, the GROOT system continuously operated and collected RO data from the GPS, Galileo, and BeiDou constellations. After mission termination, the data was recovered and processed.

3.3 | NCL Zero-Pressure Mission 1 (ZPM-1)

After the World View series of balloon flights, the NCL team focused on its internal Zero-Pressure Mission 1 (ZPM-1) during the months of September through November of 2020. While the GROOT instrument was largely tested and validated from the World View effort, other tasks were required for the preparation of an independently managed and operated HAB flight.

One major component included ballast release functionality from the BRIC system used to increase altitude during the night to combat changes in buoyancy due to the natural cooling of the atmosphere. This flight also required a multi-redundant cut-down mechanism for flight termination. Due to the many components and extended duration of operation, the total payload mass was 28.5 kg (63 lbs).

The payload mass necessitated using a zero-pressure balloon in lieu of a latex alternative due to its heavy-lift capacity. The payload configuration is shown in Figure 14. This shows the GROOT/BRIC system payloads alongside the ballast mass bladder filled with a water-glycol solution.

Figure 15 shows preparations on launch day near Empire, Nevada, on November 28, 2020. This mission required 8.5 cubic meters (300 cubic ft) of helium to achieve the necessary lift. Figure 16 shows the filling process. The balloon ascended to a maximum altitude of 31.7 km (104,567 ft) and stayed aloft for a total of 12 hours, traveling southeast to Utah as shown in Figure 17.

FIGURE 14 The NCL Zero-Pressure Balloon Mission (ZPM-1) payload

FIGURE 15 NCL Zero-Pressure Balloon Mission (ZPM-1) launch preparations

FIGURE 16 The NCL Zero-Pressure Balloon Mission (ZPM-1) balloon filling

During nightfall, ZPM-1 dropped to an altitude of 17.9 km (59,000 ft) due to colder ambient temperatures at altitude. This was lower than expected, causing the balloon to drift eastward towards the Rocky Mountains instead of the relatively flat lands of New Mexico as predicted. As such, the decision was made to end the mission after 12 hours, instead of the anticipated 36 hours, due to recovery considerations. The payload was recovered in southern Utah. A video of the mission can be viewed at https://youtu.be/fzlcCyeYcno.

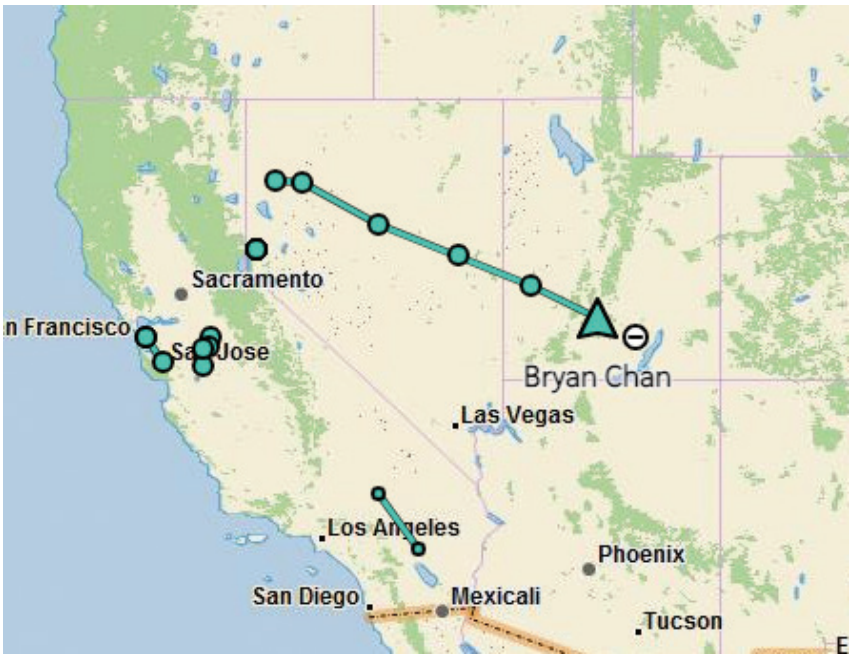

FIGURE 17 The NCL Zero-Pressure Balloon Mission (ZPM-1) trajectory

3.4 | Future Flights

The flight-testing campaigns described thus far concludes coverage of initial experiments with the GROOT system's proof of concept. Our next steps focus on the AIRO system. The first flight tests of the AIRO instrument occurred in August of 2021 on the NASA DC-8 research aircraft shown at the Armstrong Flight Research Center in California in Figure 18. The AIRO instrument was flown alongside the GROOT system for data comparison.

FIGURE 18 The NASA DC-8 research aircraft

4 | RESULTS

The focus of this paper is primarily on the hardware development and flight data collection campaigns undertaken to characterize the performance potential of COTS GNSS receivers for aerial GNSS-RO. Here we give some highlights to show significant findings, more details on the algorithms, approach, and results that will be presented in future work.

4.1 | Data Processing

After the flight data was logged, several processing steps were required to retrieve atmospheric bending angle and refractivity. The first step was to pre-process the data for later ingestion into the retrieval algorithms. Figure 19 shows this workflow. The input is raw GNSS observables, satellite ephemeris data, and balloon state (position/velocity) data. Once parsed and aligned, the first step was to compute the excess phase by subtracting the line-of-sight phase from the receiver's measured phase. Step two was receiver clock calibration in which the excess phase of the occulting GNSS satellite was smoothed by subtracting the excess phase from a high-elevation GNSS satellite. Step three was cycle slip correction in which an exponential curve was fitted to the data to both smooth and remove medium-to-large discontinuities. Step four uses a Gaussian process regression (GPR) to further remove smaller discontinuities. Finally, the processed result: RO phase, RO Doppler, RO SNR, and balloon state were exported as a NetCDF file, a format convenient for downstream GNSS-RO retrieval processing.

In order to evaluate the performance of the balloon-borne GNSS-RO retrieval algorithm, an end-to-end simulation system originally developed for aircraft-based GNSS-RO was adapted for the balloon-borne RO measurements. This algorithm was adapted from an aircraft-based RO retrieval algorithm (Xie et al., 2018) and is implemented on balloon-borne RO measurements for the first time. The algorithm is different from typical space-borne retrieval algorithms as the RO receiver was located inside the atmosphere and moving much slower compared to LEO-RO satellites. In addition, a radio-holographic retrieval module that uses a technique called full-spectrum inversion (FSI) was developed to improve the moist lower troposphere RO retrieval that encountered multipath problems that could lead to large retrieval errors in the standard retrieval methods (i.e., Geometric Optics) (Adhikari et al., 2016). The FSI retrieval is capable of retrieving the high-quality bending angle values from the complex RO phase and amplitude measurements under multipath conditions. Nelson et al. (2022) describe the balloon-borne algorithm in more detail.

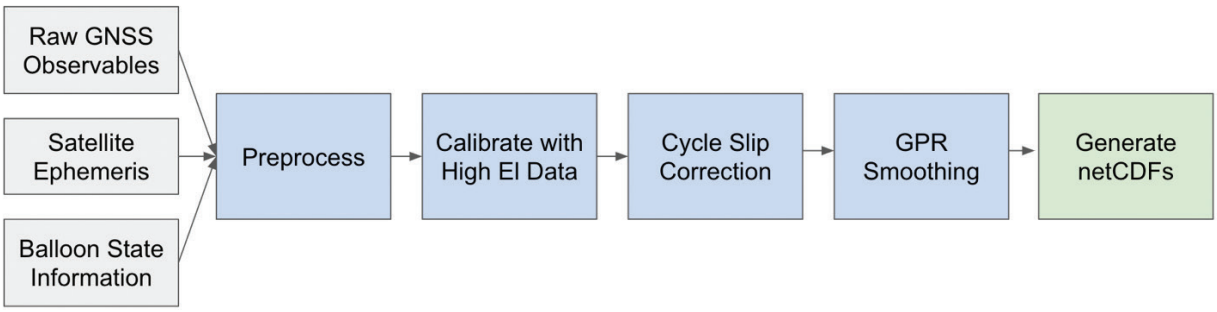

FIGURE 19 GNSS-RO data pre-processing workflow

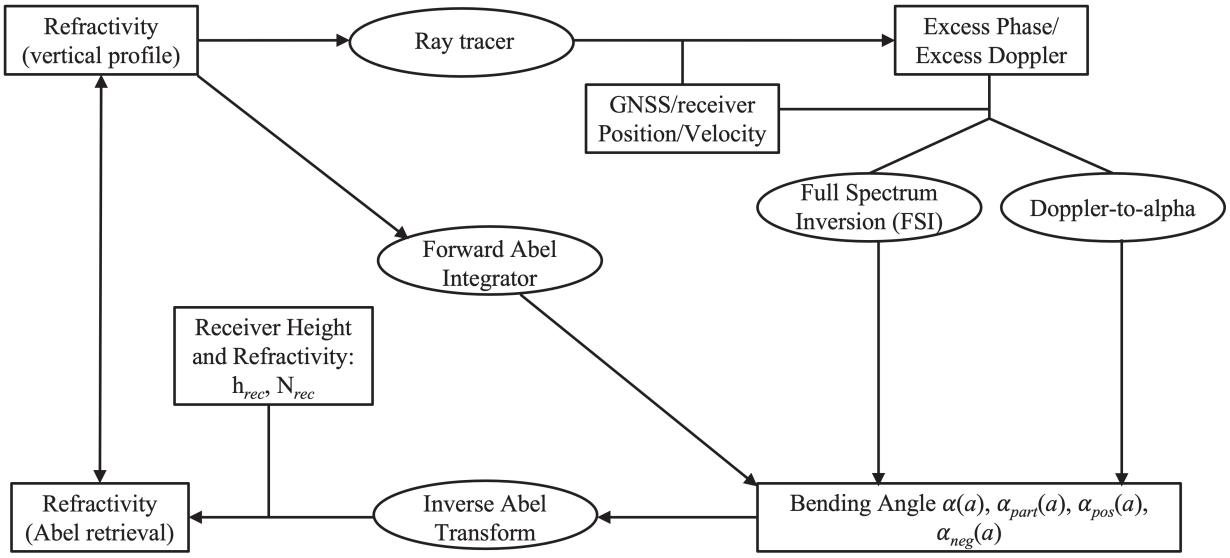

FIGURE 20 An end-to-end processing system for airborne/balloon-borne GNSS RO-simulation, retrieval, and evaluation

As shown in Figure 20, the simulation system includes four main components: (a) a Geometrical Optics (GO) ray tracer (ROSAP or radio occultation simulator for atmospheric profiling), which simulates the GNSS signal as it travels through a given atmospheric refractivity model; (b) a GO retrieval module that derives the bending angle values from excess Doppler measurements (Doppler-to-Alpha; Xie et al., 2008) and the radio-holographic retrieval module using full-spectrum inversion (Adhikari et al., 2016); (c) a forward integrator that generates the bending angle profile through the forward integration of an input 1D refractivity profile; and (d) an inverse operator to retrieve a refractivity profile via Abel inversion.

4.2 | Initial Results

In this section, we present some preliminary results from the World View flight campaign. During the 120-hour flight, the GROOT system was exposed to 680 observable setting radio occultation events from GPS, Galileo, GLONASS, and BeiDou. Of these observed RO soundings, GLONASS data was not analyzed due to its comparatively poor quality.

RO failures from the remaining constellations were due primarily to early loss-of-lock, mainly attributed to mechanical instability and radio-frequency (RF) interference of the World View stratollite platform. Another factor was that the commercial receiver and antenna combination used in this experiment seemed comparably better tuned for GPS compared to other constellations, leading to a comparatively lower quality of data for Galileo, GLONASS, and BeiDou which, therefore, more often failed quality controls.

After these issues, the remaining 195 RO soundings were successfully parsed. The data down selection in this process is summarized in the Sankey plot in Figure 21. This flight demonstrated that RO data with a very high temporal resolution could be collected using a balloon over a designated area of interest. Of these 195 RO soundings, 15 were selected for further analysis and bending angle retrieval where the median L1 excess phase of this data set was 162 m, with a median minimum elevation angle of -4.55 degrees.

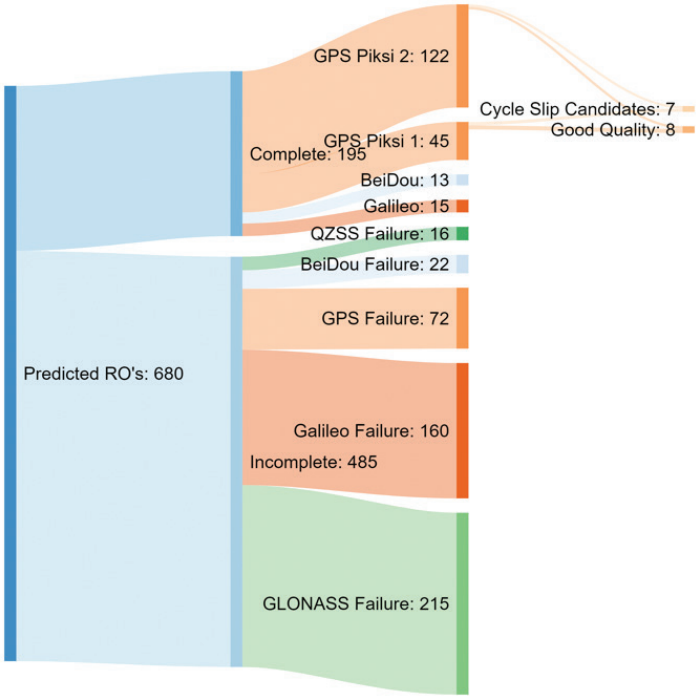

FIGURE 21 Sankey plot of RO data quality collected during the World View 5-day mission

The baseline for comparison was the European Centre for Medium-Range Weather Forecasts (ECMWF) fifth-generation reanalysis product, ERA5 (Hersbach et al., 2020). This has a horizontal resolution of 31 km on 137 levels from the surface up to 0.01 hPa (around 80 km). Applying the balloon RO retrieval algorithm on this data showed very good agreement between the balloon-borne RO measurements (excess phase/Doppler and bending angle values) compared to the close-coincident ERA5 profile.

Figure 22 shows this agreement for a specific case involving GPS PRN 32. In the top-right plot of Figure 22, raw Doppler observables were not plotted because only smoothed Doppler was used for further processing and analysis. Figure 23 shows the median refractivity bias between 13 World View balloon RO soundings and the ERA5 model. This shows agreement generally within 5% which shows much promise for operational deployment. This shows good agreement above ~ 4.5 km, although some biases do emerge at lower altitudes.

It is worth noting that the Piksi receiver is capable of tracking the RO signal deep into the lower troposphere close to ~ 3 km above the surface. Generally, high quantities of continuous RO retrievals from the lower stratosphere (~ 18 km) down to the mid-troposphere (~ 5 km) would be needed to measurably improve weather monitoring globally. RO measurements further down to the planetary boundary layer (2 to 3 km) in the tropics and subtropics are even more valuable to improve the forecasting of tropical storm intensity and trajectory (Ao et al., 2012; Xie et al., 2012). In specific applications such as tropical cyclones, the boundary layer height is less than 1 km due to vortex compression (Nelson et al., 2021; Ren et al., 2020; Shi et al., 2021).

Figure 24 shows the trajectory of the first 5-day World View flight alongside the GNSS-RO profile locations. This showcases an ability to deploy such a system for persistent data collection over a local area of interest. The balloon platform showcased station-keeping ability and generally remained in Arizona airspace.

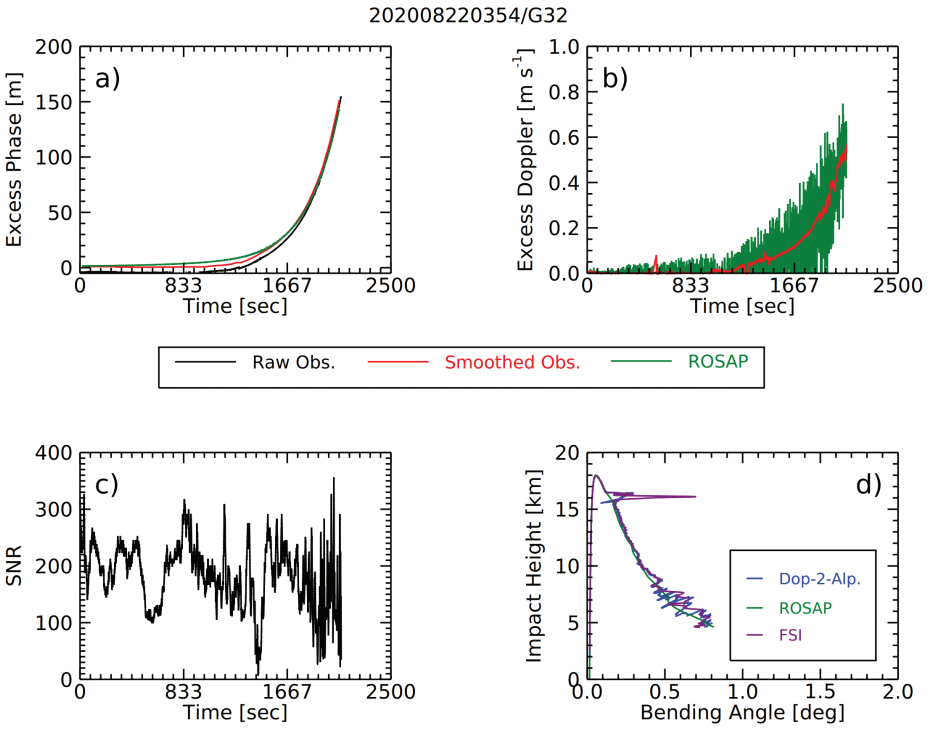

FIGURE 22 The G32 balloon-borne RO recorded August 22, 2020; (Top-left) the excess phase and (top-right) excess Doppler and simulation; (bottom-left) the L1 SNR and (bottom-right) the bending angle profiles from simulation (green), GO retrieval (blue), and FSI retrieval (purple)

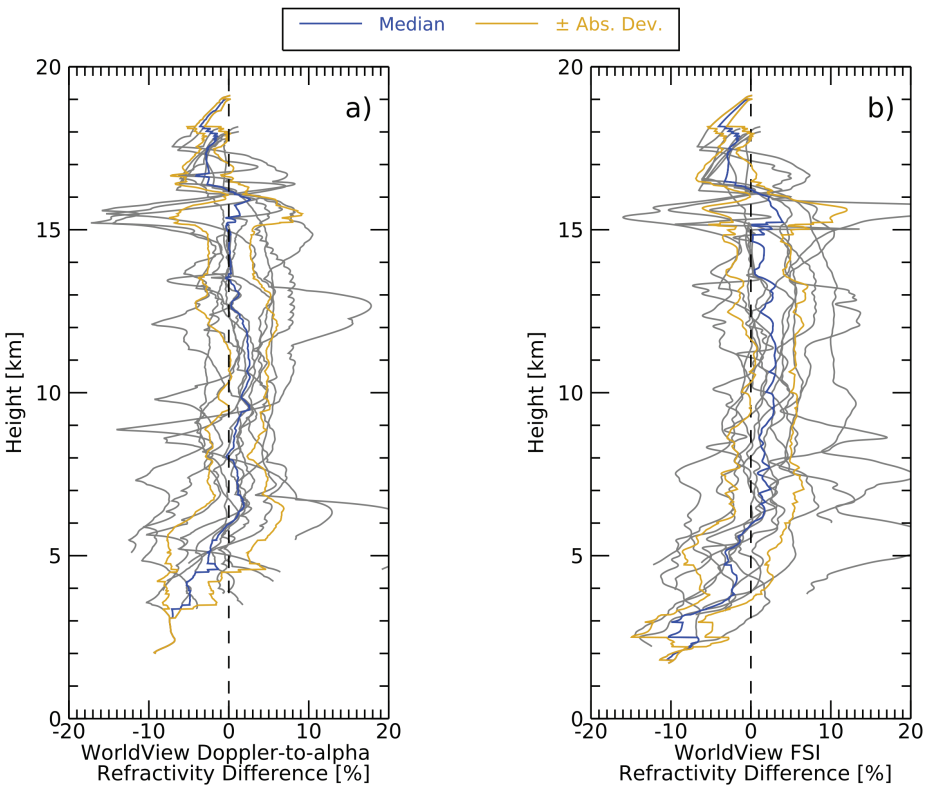

FIGURE 23 Median refractivity bias between World View balloon retrievals and the standard ERA5 model; median biases were within 5% for the majority of the profile

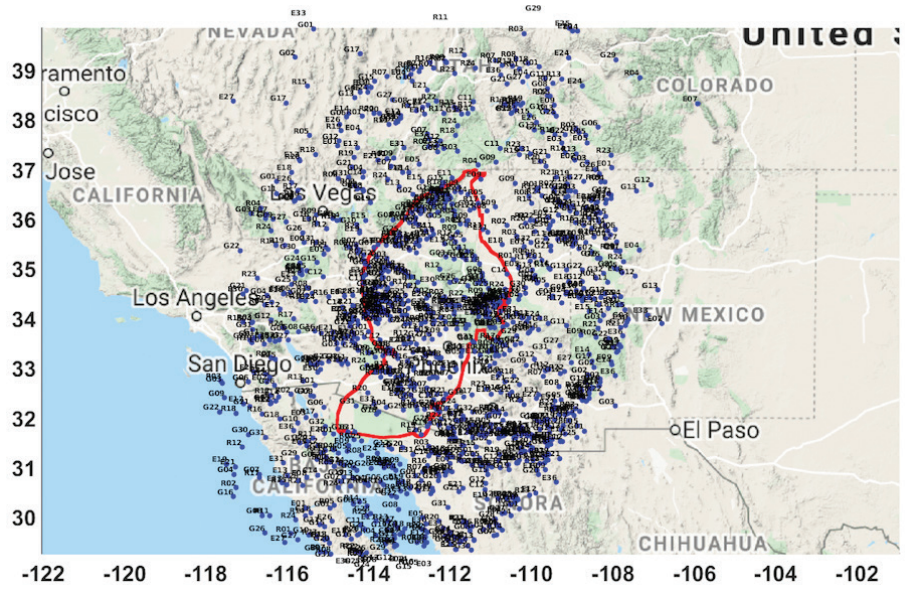

FIGURE 24 GNSS-RO soundings recorded on a 5-day high-altitude balloon flight

Over 1,350 RO events occurred within an area of 900 km x 1000 km. This represents 680 setting satellites and 670 rising. The temporal RO sounding density, typically defined as daily RO soundings per million square miles, exceeded 340 RO soundings/10^6 miles^2 (130 RO soundings/10^6 km^2) for this single balloon flight, compared to approximately 50 from all operational space-based RO sources available in 2020. This represents a nearly sevenfold increase.

5 | CONCLUSION

This paper describes a multi-year effort to develop a low-cost and scalable approach to aerial (aircraft/balloon) GNSS-RO based on COTS GNSS receivers. We presented hardware prototypes and data processing techniques, demonstrating the technical feasibility of the approach through results from several flight testing campaigns. This represents more than 150 hours of data collection from both fixed-wing aircraft and high-altitude balloons.

The primary scientific instrument described here is the GNSS Radio Occultation and Observable Truth (GROOT) system based on COTS-only GNSS receivers with closed-loop tracking. We demonstrated unprecedented temporal and spatial sampling density through balloon station-keeping and balloon-borne RO retrieval algorithms. Combined, these flight tests demonstrate that aerial platforms (e.g., balloons, aviation) are an attractive method for retrieving RO soundings over regional areas of interest for operational weather data collection.

Preliminary results are shown from a multi-day high-altitude balloon flight test over the western United States, wherein several hundred GNSS-RO soundings were collected. Station-keeping allowed for GNSS-RO soundings with high spatial and temporal resolution, resulting in a nearly sevenfold increase in RO sounding density compared to all operational space-based RO sources combined. Using balloon-borne retrieval algorithms, bending angles and refractivities were retrieved and matched standard models to within 5%. Furthermore, this system proved capable of signal tracking down to the planetary boundary layer (2 to 3 km).

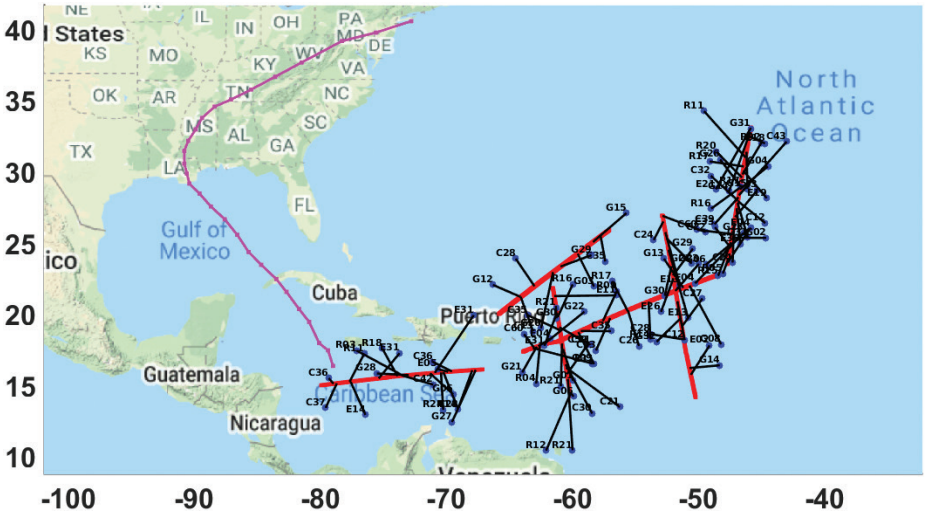

FIGURE 25 GNSS-RO soundings (with ray paths in black) collected by the AIRO system from the NASA DC-8 flight test campaign, which coincided with Hurricane Ida (purple) in August 2021.

Looking forward, we expect the next-generation instrument known as the Aircraft In-situ and Radio Occultation (AIRO) device to perform even better with a smaller form factor. Initial tests were flown in August of 2021 on a NASA DC-8 research aircraft. A unique aspect of this test campaign was that it was located in the tropics where hurricanes and tropical storms originate. During the week of August 24, the AIRO instrument observed RO soundings in the Caribbean Sea and Atlantic Ocean while Hurricane Ida was forming (see Figure 25). With more analysis, we anticipate such GNSS-RO data may augment current hurricane/tropical weather monitoring and forecasting capabilities.

The larger question surrounding these efforts is whether this method of delivering balloon-borne GNSS-RO data is programmatically and commercially viable. With sufficient engineering effort, we believe that, at scale, a deck-of-cards-sized GNSS-RO sensor could be manufactured for less than $1,000 with a mass of less than 1 kg. This lightweight sensor could be integrated into long-duration balloon flights as a rideshare payload and deliver GNSS-RO data. However, especially with the recent end of Google Loon, there are a limited number long-duration balloon flights every year which inhibits the economies-of-scale benefits. Additionally, challenges remain with integrating onto existing radiosonde platforms, as the mass requirement is closer to 100 g.

As an adjacent technological development, we believe there is much promise in delivering airborne GNSS-RO data in commercial aviation applications. A similarly sized sensor could be more easily integrated onto a commercial aircraft. This sensor could tap into an existing GNSS signal and leverage the existing radio transmission system to broadcast GNSS-RO soundings to a data center in a timely fashion (< 20 minutes). Additionally, tens of thousands of aircraft fly every day which immediately resolves the scaling issues of this technology.

ACKNOWLEDGEMENTS

This work was supported by the National Oceanic and Atmospheric Administration (NOAA), National Aeronautics and Space Administration (NASA), and Airbus Silicon Valley.

REFERENCES

Adhikari, L., Xie, F., & Haase, J. S. (2016). Application of the full spectrum inversion algorithm to simulated airborne GPS radio occultation signals. *Atmospheric Measurement Techniques*, *9*(10), 5077–5087. https://doi.org/10.5194/amt-9-5077-2016

Anthes, R. A., Bernhardt, P. A., Chen, Y., Cucurull, L., Dymond, K. F., Ector, D., Healy, S. B., Ho, S. -P., Hunt, D. C., Kuo, Y. -H., Liu, H., Manning, K., McCormick, C., Meehan, T. K., Randel, W. J., Rocken, C., Schreiner, W. S., Sokolovskiy, S. V., Syndergaard, S., … Zeng, Z. (2008). The COSMIC/Formosat-3 mission: Early results. *Bulletin of the American Meteorological Society*, *89*(3), 313–333. https://doi.org/10.1175/BAMS-89-3-313

Ao, C. O., Waliser, D. E., Chan, S. K., Li, J. -L., Tian, B., Xie, F., & Mannucci, A. J. (2012). Planetary boundary layer heights from GPS radio occultation refractivity and humidity profiles. *Journal of Geophysical Research: Atmospheres*, *117*(D16). https://doi.org/10.1029/2012JD017598

Carroll, J., Chan, B., Harner, C., Reid, T., Tarantino, P., & Yu, C. Y. T. (2011). Commercial GPS in the stratosphere: cell phone GPS receiver performance on a high altitude weather balloon. *Proc. of the 24th International Technical Meeting of the Satellite Division of the Institute of Navigation (ION GNSS 2011),* Portland, OR. https://www.ion.org/publications/abstract.cfm?articleID=9881

Chan, B. C., Goel, A., Reid, T., Snyder, C., & Tarantino, P. (2019). Measuring and assessing GNSS radio occultation (GNSS-RO) profiles from balloon platforms. *American Meteorological Society 99th Annual Meeting,* Phoenix, AZ. https://ams.confex.com/ams/2019Annual/webprogram/Paper353545.html

Chan, B. C., Goel, A., Reid, T. G. R., Snyder, C. R., & Tarantino, P. M. (2018). Measuring GNSS radio occultation (GNSS-RO) profiles using high altitude balloons. *American Geophysical Union Fall Meeting.* https://ui.adsabs.harvard.edu/abs/2018AGUFM.P53A..09C/abstract

Bowler, N. E. (2020). An assessment of GNSS radio occultation data produced by Spire. *Quarterly Journal of the Royal Meteorological Society*, *146*(733), 3772–3788. https:/doi.org/10.1002/qj.3872

Feltz, M. L., Knuteson, R. O., & Revercomb, H. E. (2017). Assessment of COSMIC radio occultation and AIRS hyperspectral IR sounder temperature products in the stratosphere using observed radiances. *Journal of Geophysical Research: Atmospheres*, *122*(16), 8593–8616. https://doi.org/10.1002/2017JD026704

Haase, J. S., Maldonado-Vargas, J., Rabier, F., Cocquerez, P., Minois, M., Guidard, V., Wyss, P., & Johnson, A. V. (2012). A proof-of-concept balloon-borne Global Positioning System radio occultation profiling instrument for polar studies. *Geophysical Research Letters, 39*(2). https://doi.org/10.1029/2011GL049982

Hersbach, H., Bell, B., Berrisford, P., Hirahara, S., Horányi, A., Muñoz-Sabater, J., Nicolas, J., Peubey, C., Radu, R., Schepers, D., Simmons, A., Soci, C., Abdalla, S., Abellan, X., Balsamo, G., Bechtold, P., Biavati, G., Bidlot, J., Bonavita, M., … Thépaut, J. -N. (2020). The ERA5 global reanalysis. *Quarterly Journal of the Royal Meteorological Society*, *146*(730), 1999–2049. https://doi.org/10.1002/qj.3803

Irisov, V., Duly, T., Nguyen, V., & Masters, D. (2020). Radio occultation atmospheric profiling from the Spire nanosatellite constellation and its impact on weather forecasting. In A. Comerón, E. I. Kassianov, K. Schäfer, R. H. Picard, K. Weber, & U. N. Singh (Eds.), *Remote sensing of clouds and the atmosphere XXV* (Vol. 11531). SPIE Digital Library. https://doi.org/10.1117/12.2574128

Kahr, E., Bradbury, L., O'Keefe, K. P. G., & Skone, S. (2013). Design and operation of the GPS receiver onboard the CanX-2 nanosatellite. *NAVIGATION, 60*(2), 143–156. https://doi.org/10.1002/navi.36

Kahr, E., Montenbruck, O., O'Keefe, K., Skone, S., Urbanek, J., Bradbury, L., & Fenton, P. (2011). GPS tracking of a nanosatellite –– the CANX-2 flight experience. *8th International ESA Conference on Guidance, Navigation, and Control Systems.* https://schulich.ucalgary.ca/labs/position-location-and-navigation/files/position-location-and-navigation/kahr2011_conference.pdf

Kumar, M. (2006). New satellite constellation uses radio occultation to monitor space weather. *Space Weather*, *4*(5). https://doi.org/10.1029/2006SW000247

Kuo, Y. -H., Schreiner, W. S., Wang, J., Rossiter, D. L., & Zhang, Y. (2005). Comparison of GPS radio occultation soundings with radiosondes. *Geophysical Research Letters*, *32*(5). https://doi.org/10.1029/2004GL021443

Nelson, K. J., Xie, F., Ao, C. O., & Oyola-Merced, M. I. (2021). Diurnal variation of the planetary boundary layer height observed from GNSS radio occultation and radiosonde soundings over the southern great plains. *Journal of Atmospheric and Oceanic Technology*, *38*(12), 2081–2093. https://doi.org/10.1175/JTECH-D-20-0196.1

Nelson, K. J., Xie, F., C., C. B., Goel, A., Kosh, J., Reid, T. G. R., … Soedarmadji, W. (2022). GNSS radio occultation retrievals using commercial off-the-shelf receivers on a balloon payload [Manuscript submitted for publication]. *Atmospheric Measurement Techniques (AMT).* https://doi.org/10.5194/amt-2022-198

Ren, Y., Zhang, J. A., Vigh, J. L., Zhu, P., Liu, H., Wang, X., & Wadler, J. B. (2020). An observational study of the symmetric boundary layer structure and tropical cyclone intensity. *Atmosphere*, *11*(2). https://doi.org/10.3390/atmos11020158

Sa'd, J. (2020). *mosaicHAT: An open source GNSS HAT for Raspberry PI.* https://github.com/septentrio-gnss/mosaicHAT

Sarda, K., Grant, C., Eagleson, S., Kekez, D., Shah, A., & Zee, R. (2009). Canadian Advanced Nanospace Experiment 2 orbit operations: one year of pushing the nanosatellite performance envelope. *Small Satellite Conference*. https://digitalcommons.usu.edu/smallsat/2009/all2009/24

Schreiner, W. S., Weiss, J. P., Anthes, R. A., Braun, J., Chu, V., Fong, J.,Hunt, D., Kuo, Y. -H., Meehan, T., Serafino, W., Sjoberg, J., Sokolovskiy, S., Talaat, E., Wee, T. K., & Zeng, Z. (2020). COSMIC-2 radio occultation constellation: first results. *Geophysical Research Letters*, *47*(4). https://doi.org/10.1029/2019GL086841

Shi, J., Zhang, K., Wu, S., Shi, S., & Shen, Z. (2021). Investigation of the atmospheric boundary layer height using radio occultation: A case study during twelve super typhoons over the northwest pacific. *Atmosphere*, *12*(11). https://doi.org/10.3390/atmos12111457

Shume, E. B., Komjathy, A., Langley, R. B., Verkhoglyadova, O., Butala, M. D., & Mannucci, A. J. (2015). Intermediate-scale plasma irregularities in the polar ionosphere inferred from GPS radio occultation. *Geophysical Research Letters*, *42*(3), 688–696. https://doi.org/10.1002/2014GL062558

Skone, S., Swab, M., Platzer, P., Johl, S., & Cappaert, J. (2014). GNSS radio occultation methods for CubeSat missions: The University of Calgary and Spire partnership. *American Geophysical Union Fall Meeting*. https://ui.adsabs.harvard.edu/abs/2014AGUFM.A23I3353S/abstract

Swab, M. (2015). *Sounding of the ionosphere using the CanX-2 nano-satellite and single-frequency radio occultation techniques* [Master's thesis, University of Calgary]. http://doi.org/10.11575/PRISM/27833

Ware, R., Exner, M., Feng, D., Gorbunov, M., Hardy, K., Herman, B., Kuo, Y., Meehan, T., Melbourne, W., Rocken C., Schreiner, W., Sokolovskiy, S., Solheim, F., Zou, X., Anthes, R., Businger, S., & Trenberth, K. (1996). GPS sounding of the atmosphere from low Earth orbit: Preliminary results. *Bulletin of the American Meteorological Society*, *77*(1), 19–40. https://doi.org/10.1175/1520-0477(1996)077<0019:GSOTAF>2.0.CO;2

Werner, D. (2020). NOAA signals strong appetite for radio occultation. *Space News.* https://spacenews.com/radio-occultation-ams-2020

Xie, F., Adhikari, L., Haase, J. S., Murphy, B., Wang, K. -N., & Garrison, J. L. (2018). Sensitivity of airborne radio occultation to tropospheric properties over ocean and land. *Atmospheric Measurement Techniques*, *11*(2), 763–780. https://doi.org/10.5194/amt-11-763-2018

Xie, F., Haase, J. S., & Syndergaard, S. (2008). Profiling the atmosphere using the airborne GPS radio occultation technique: A sensitivity study. *IEEE Transactions on Geoscience and Remote Sensing*, *46*(11), 3424–3435. https://doi.org/10.1109/TGRS.2008.2004713

Xie, F., Wu, D. L., Ao, C. O., Mannucci, A. J., & Kursinski, E. R. (2012). Advances and limitations of atmospheric boundary layer observations with GPS occultation over southeast Pacific Ocean. *Atmospheric Chemistry and Physics*, *12*(2), 903–918. https://doi.org/10.5194/acp-12-903-2012

Yue, X., Schreiner, W. S., Hunt, D. C., Rocken, C., & Kuo, Y. -H. (2011). Quantitative evaluation of the low Earth orbit satellite based slant total electron content determination. *Space Weather*, *9*(9). https://doi.org/10.1029/2011SW000687

Yue, X., Schreiner, W. S., Pedatella, N., Anthes, R. A., Mannucci, A. J., Straus, P. R., & Liu, J. -Y. (2014). Space weather observations by GNSS radio occultation: From FORMOSAT-3/COSMIC to FORMOSAT-7/COSMIC-2. *Space Weather*, *12*(11), 616–621. https://doi.org/10.1002/2014SW001133

How to cite this article: Reid, T., Chan, B., Goel, A., Kosh, J., Snyder, C., Tarantino, P., Soedarmadji, S., Soedarmadji, W., Nelson, K., Xie, F., & Vergallo, M. (2022) Commercial GNSS radio occultation on aerial platforms with off-the-shelf receivers. *NAVIGATION, 69*(4). https://doi.org/10.33012/navi.544